Endothelial Slit2 guides the Robo1-positive sympathetic innervation during heart development

Juanjuan Zhao[1], PhD; Susann Bruche[1,2], PhD; Konstantinos Lekkos[1,2], MSc; Carolyn Carr[1], PhD; Joaquim M. Vieira[3], PhD; John G. Parnavelas[4], PhD; William D. Andrews[4], PhD; Mathilda T.M. Mommersteeg, PhD[1,2] ✉

[1] Department of Physiology, Anatomy & Genetics, University of Oxford, Oxford, UK
[2] Institute of Developmental and Regenerative Medicine, Old Road Campus, University of Oxford, Oxford, UK
[3] School of Cardiovascular & Metabolic Medicine & Sciences, Faculty of Life Sciences & Medicine, Kings College London, British Heart Foundation Centre – James Black Centre, London, UK.
[4] Department of Cell and Developmental Biology, University College London, London, UK.

Short title: Slit-Robo signalling in cardiac innervation development

✉ Corresponding author:

Mathilda T.M. Mommersteeg

Institute of Developmental and Regenerative Medicine

Department of Physiology, Anatomy and Genetics

University of Oxford

Old Road Campus, Roosevelt Drive

Oxford OX3 7TY

United Kingdom

Word count: 1525

Abstract

Axon guidance cues direct nerves in the heart during development, disease and regeneration. These cues determine cardiac innervation patterning by regulating the balance between chemo-attraction and chemo-repulsion. However, the role of one of the most crucial ligand-receptor combinations among axon guidance molecules, the Slit chemo-active ligands and their Roundabout (Robo) transmembrane receptors, remains unknown during cardiac innervation patterning. To test if Slit-Robo signalling is important for cardiac innervation guidance, we analysed Slit and Robo mouse knock-outs. Constitutive *Slit2*$^{-/-}$ ventricles showed significantly reduced innervation, while *Slit3*$^{-/-}$ hearts showed temporary increased levels of innervation compared to wild-type littermate controls. Whereas innervation was not affected in *Robo2*$^{-/-}$ mice, the phenotype seen in *Slit2*$^{-/-}$ ventricles was recapitulated in *Robo1*$^{-/-}$ mice. Detailed expression analysis identified expression of Slit2 ligand in the endothelium of the coronary vessels, while Slit3 was highly present in the coronary smooth muscle wall and in the innervation. Both the Robo1 and Robo2 receptors were present in the nerves and at low levels in the vessels. Knocking out *Slit2* specifically in the endothelium recapitulated the defects seen in the constitutive *Slit2*$^{-/-}$ hearts. *Ex vivo* axon guidance cultures showed that attraction of axons extending from the ganglia was strongly reduced in ventricles with absence of endothelial Slit2 compared to wild-type controls. In absence of endothelial Slit2, adult mice showed reduced response to challenging the sympathetic innervation. In conclusion, we have identified an important new chemo-active Slit2-Robo1 pathway required for correct cardiac innervation development.

52 **Introduction**

53 A number of recent studies have revealed the extent and importance of the innervation of the
54 heart during disease, regeneration and aging. [1–5] Alterations in the innervation play a role in
55 the susceptibility to arrhythmias in various cardiac diseases, from cardiac ganglia in the
56 pathogenesis of atrial fibrillation, to ventricular nerves in the predilection toward ventricular
57 arrhythmias and sudden cardiac death in myocardial scar areas, chronic congestive heart failure,
58 diabetic neuropathy and diseases such as Long QT and Brugada syndrome.[2,6–11]

59 Previous studies have shown that neurogenic genes including Semaphorin3a (Sema3a)
60 and its receptor Neuropilin1 (Nrp1), Nerve Growth Factor (NGF), glial cell line-derived
61 neurotrophic factor (GDNF), Edn1 and its receptor Ednra as well as Plexin A4 are involved in
62 determining cardiac innervation patterning during development by regulating the balance
63 between chemo-attraction and chemo-repulsion.[12–18] Some of these pathways are re-activated
64 during aging as accumulation of senescent cells stimulates the release of Sema3a from the
65 coronary vasculature, reducing innervation density in the heart. Tipping the balance towards
66 chemo-repulsive Sema3a and inducing denervation increases the risk of arrhythmias in the
67 aging heart, which is reversible with senolytic drugs.[5] This shows that even after birth,
68 maintaining the balance between chemo-attraction and repulsion remains important throughout
69 life and targetable with therapeutics.

70 Only a relatively small number of attractive or repulsive axon guidance cues are known
71 and while we now know the involvement of key guidance factors in the heart, knowledge on
72 one major player is still lacking. Here, we report a crucial novel role for the Slit-Robo signalling
73 pathway in cardiac innervation guidance during development. The Roundabout (Robo)
74 transmembrane receptors and their Slit ligands were first studied for their role in axonal
75 guidance in the embryonic nervous system.[19] However, many new roles have been identified
76 since, especially in cancer and embryogenesis.[19,20] In the mammalian heart, the pathway is

involved in cardiac chamber formation, cardiac neural crest migration and adhesion, the development of the pericardium and caval veins, membranous ventricular septum and valve formation.[21–24] Here, using constitutive and conditional knock-out approaches, axon guidance experiments and functional analysis, we show that interaction of Slit2 and Robo1 is important for correct innervation patterning during heart development. This knowledge will help us better understand the mechanisms underling dysregulation of innervation during development, aging and disease and how to promote appropriate nerve growth.

Methods and Data Availability

Mouse lines

All experiments were performed in accordance with the UK Animals (Scientific Procedures) Act 1986 and institutional guidelines. *Robo1*^{tm1Wia} [25] and *Robo2*^{tm1Rilm} [26] were obtained from William Andrews (UCL, London, UK). *Robo1*^{tm1Matl}*;Robo2*^{tm1Rilm},[27] Slit1^{tm1Matl} and Slit2^{tm1Matl},[28] *Slit2*$^{tm1.1Ics}$ [29] from Alain Chedotal (Institut de la Vision, Paris, France). Slit3$^{tm1.1Dor}$ [30] from David Ornitz. [20]*Tg(Wnt1-cre)*^{11Rth},[31] *Tg(Tek-cre)*^{12Flv} (*Tie2-cre*)[32] and *Tg(Myh6-cre/Esr1*)*^{1Jmk} [33] were obtained from the Jackson lab. All lines were maintained on a C57/BL6J background (C57BL/6JOlaHsd, model code 057, Envigo). The day the vaginal plug was found was considered as embryonic day (E) 0.5. Cre allele *Tg(Myh6-cre/Esr1*)*^{1Jmk} was induced by oral gavage with five consecutive doses of 20mg/kg 4-hydroxytamoxifen (Sigma, T5648) at E12.5 to E16.5.

Tissue processing and immunohistochemistry-paraffin section staining

Fluorescent immunohistochemistry was performed as previously described.[34] Embryos were dissected and fixed overnight in 4% paraformaldehyde (ChemCruz, SC-281692). Following a brief wash in PBS (Gibco, 18912-014), the samples were dehydrated using an ethanol gradient (two-hour incubations in 70%, 80%, 90% and 96% and two 1-hour incubations in 100% ethanol, Sigma-Aldrich, 32221-2.5L-M)) before being incubated in 1-butanol (MP biomedicals, 194001) at room temperature overnight. Before mounting the embryos in sectioning moulds, three two-hour incubations were performed in paraffin (Paraplast plus, Sigma-Aldrich, P3683) at 65°C. Using a Leica microtome (Microm HM325), 10µm sections were collected, mounted on Superfrost Plus glass slides (VWR, 631-0108) ensuring even

108 coverage of the heart (one in every three sections per staining combination) and were allowed
109 to dry overnight at 33°C.

110 The slides were de-waxed in Xylene (Fisher Scientific, X/0200/17) twice for 5 min and
111 rehydrated in an ethanol gradient (100%, 100%, 96%, 90%, 80%, 70%) for one minute each
112 before being incubated for one more minute in PBS. The samples were then boiled for 4 min
113 in a pressure cooker in antigen unmasking solution (H-3300, Vector Laboratories) and were
114 allowed to cool down in PBS-T (Tween-20 0.1%, Chemcruz, sc-29113) before a ring was
115 drawn around them using an ImmEdge pen (Vector Laboratories, H4000). The sections were
116 blocked for 30 min at room temperature in a humidified chamber using blocking reagent [0.5%
117 blocking reagent powder (Akoya Bioscience, FP1012), 0.15 M NaCl, 0.1 M Tris-HCl (pH 7.5)]
118 and were then incubated with primary antibody diluted blocking solution overnight at room
119 temperature. Following three 5min washes in PBS-T, the secondary antibody was applied
120 (1:200 in blocking solution, Invitrogen, Alexa range) for 2 hours at room temperature.

121 For the Slit and Robo antibodies, an additional amplification step was added to enhance
122 the signal using the TSA kit (NEL756001KT, Perkin and Elmer). Instead of an Alexa
123 secondary antibody, a biotinylated secondary antibody was used at a 1:200 dilution in blocking
124 solution for 45 min at room temperature, followed by three 5 min washes in PBS-T prior to a
125 30 min incubation with conjugated Streptavidin-Horse Radish Peroxidase (Vector
126 Laboratories, SA-5004) and then three 5 min washes in PBS-T. Either fluorescein or
127 tetramethylrhodamine (in DMSO, NEL756001KT) diluted at 1:100 in amplification buffer was
128 then added to the sections for 3 min, followed by three 5 min washes with PBS and staining
129 with DAPI (2.5 µg/ml, Sigma, MBD0015). Mowiol 4-88 (Applichem, A9011,1000) was used
130 to mount the slides, which were cured at 37°C in the dark. Primary antibodies against the
131 following proteins were used: goat polyclonal anti-cardiac Troponin I (cTnI, 1:200; Hytest Ltd,
132 4T21/2), mouse monoclonal anti-Myosin heavy chain (MF20, 1:50, HSHB, AB-2147781),

133 rabbit polyclonal anti-Peripherin (Prph, 1:200; Millipore, AB1530), rabbit polyclonal anti-
134 Tyrosine Hydroxylase (TH, 1:200; Millipore, AB152), goat polyclonal anti-Robo1 (1:200;
135 R&D Systems, AF1749), goat polyclonal anti-Robo2 (1:200; R&D Systems, AF3147), sheep
136 polyclonal anti-Slit2 (1:200; R&D Systems, AF5444), rat monoclonal anti-Slit3 (1:200; R&D
137 Systems, MAB3629), rabbit polyclonal anti-Erg1 (1:200, Abcam, ab110639) and rabbit
138 polyclonal anti-Smooth muscle myosin heavy chain 11 (Myh11, 1:200, Abcam, ab125884).
139 Imaging was performed on a Nikon microscope (Nikon, Eclipse Ci-L). Images were processed
140 using ImageJ to generate magenta and green colour combinations.[35]
141
142 **Volume measurements**
143 To quantitate the nerve density in the ventricle, every third transverse 10 µm section capturing
144 the entire diameter of the heart was stained as detailed above for cTnI and Peripherin or TH
145 and imaged using a Nikon microscope (Nikon, Eclipse Ci-L). The images were loaded into 3D
146 reconstruction software (Amira 6.3.0, Thermo Fisher Scientific). Images were resampled,
147 aligned and different labels were created for the myocardium of the ventricle based on cTnI
148 thresholding and for the innervation surrounding the ventricle, based on Peripherin
149 thresholding for total innervation or based on TH thresholding for sympathetic innervation. All
150 ventricular innervation was included, epicardial and intramyocardial. The label data was used
151 to generate volume information for the myocardium of the ventricle and innervation. To
152 measure the coronary vessels, similar volume measurements were performed for the lumen of
153 the coronary vasculature. Measurements were performed blind and no animals were excluded.
154 For controls we used Cre-negative hetero- and homozygous floxed littermates as well as Cre-
155 positive mice that had not inherited floxed alleles.
156
157 **Immunohistochemistry-whole mount staining**

158 Mouse hearts were prepared and fixed as described above and subsequently dehydrated by
159 methanol series (50-100%) and bleached overnight in 6% H_2O_2 in methanol. Hearts were then
160 re-hydrated, blocked in PBSGT blocking buffet (0.2% gelatin (Sigma, G7041), 0.5% Triton X-
161 100 (Merck, T8787) and 0.01% thimerosal in PBS) for 2-4 days. Primary antibodies were
162 diluted in PBSGT as follows: goat polyclonal anti-cardiac Troponin I (cTnI, 1:200; Hytest Ltd,
163 4T21/2), rabbit polyclonal anti-Tyrosine Hydroxylase (TH, 1:200; Millipore, AB152). Hearts
164 were incubated in primary antibodies at 37°C for 1 week. Afterwards, the hearts were washed
165 six times with PBSGT at room temperature before secondary antibody incubation in PBSGT
166 for 2 days. Subsequently, the hearts were washed six times for 1 hour in PBSGT. The hearts
167 were then dehydrated in a graded tetrahydroflurane (THF, Sigma-Aldrich, 186562) series
168 (50%, 80%, and 100%) and delipidated in dichloromethane (DCM, Sigma-Aldrich, D65100).
169 Finally, samples were incubated in dibenzyl ether (DBE, Sigma-Aldrich, 108014) until clear
170 and stored in DBE at room temperature. Samples were imaged on a light-sheet microscope
171 (Zeiss, lightsheet Z.1). 3D-rendered images were visualized and captured with Imaris software
172 (Bitplane, Version 7.6.4).
173
174 **Explant co-cultures**
175 Ventricles and stellate ganglia (STG) were dissected out from E14.5 or E15.5 mouse embryos
176 with the indicated genotype, placed in PBS and cut into pieces and plated into a three-
177 dimensional collagen matrix (3D collagen cell culture system, Chemicon) concurrently in
178 DMEM media containing 15% fetal bovine serum (FBS, Sigma, F7524) for three days. The
179 ventricle was placed 300-500μm away from the STG. Myocardium and neurite outgrowth were
180 visualised by immunostaining whole-mount explants with rabbit polyclonal anti-Peripherin
181 (1:200; Millipore, AB1530) and goat polyclonal anti-cardiac Troponin I (cTnI, 1:200; Hytest
182 Ltd, 4T21/2), followed by immunofluorescence detection using Alexa Fluor secondary

183 antibodies. For quantitative analysis of the extent of axon growth from the STG into the heart,
184 fluorescence images were captured at 4µm steps by using a spinning disk confocal microscope
185 (PE Ultraview spinning disk). These pictures were projected over the Z axis and then merged
186 manually using Volocity software (Quorum Technologies Inc.). STG explants were divided
187 into forward and backward portions from the centre. The axons growing toward the ventricles
188 were measured using 3D reconstruction software (Amira 6.3.0, Thermo Fisher Scientific).
189
190 **Electrocardiography (ECG) studies**
191 ECG recording of heart rate (HR) was acquired with MouseMonitor software (INDUS
192 instruments). 2-3 months old male mice were anaesthetized with 1.5% isoflurane (IsoFlo
193 Zoetis) in oxygen and kept at a constant 37° temperature using a heating pad for the duration
194 of analysis. Following baseline reading, mice were challenged by isoproterenol (Acros,
195 14190250, 0.5 mg/kg by intraperitoneal injection).
196
197 **Statistics**
198 Detailed statistics and p-values are indicated in the figure legends. T-test or one-way ANOVA
199 with Tukey's Test have been applied as indicated. Minimum to maximum box-violin plots are
200 shown with all data points.
201
202

203 **Results**

204

205 **Constitutive knock-out analysis indicates a role for Slit2 and Robo1 during cardiac**
206 **innervation development**

207 To test if Slit-Robo signalling is important for cardiac innervation guidance, we first analysed
208 constitutive mouse knock-outs for ventricular innervation at embryonic day (E)14.5/E15.5 and
209 E18.5 using Peripherin to label the total innervation (Figure 1A-B). *Slit1*$^{-/-}$ hearts did not show
210 a phenotype at E14.5, but *Slit2*$^{-/-}$ hearts showed significantly reduced ventricular innervation.
211 While *Slit3*$^{-/-}$ hearts showed increased levels of innervation compared to wild-type littermate
212 controls at E14.5, this difference was not significant anymore at E18.5. Whereas the
213 innervation was not affected in *Robo2*$^{-/-}$ mutants, the phenotype seen in *Slit2*$^{-/-}$ hearts was
214 recapitulated in *Robo1*$^{-/-}$ hearts at E14.5 and still present at E18.5. Simultaneously knocking
215 out *Robo1* and *Robo2* did not further increase the defects seen in the single *Robo1*$^{-/-}$ hearts at
216 E15.5. We confirmed that these results were not influenced by differences in ventricular
217 volume between the mutants and wild-type controls (Figure 1C). This data indicates a role for
218 Slit2 and Robo1 during cardiac innervation development.

219

220 **The coronary endothelium acts as a source of chemo-attractive Slit2 that guides the**
221 **Robo1-positive nerves during heart development**

222 Previously we have shown expression of the different Slit ligands and Robo receptors in cell-
223 types such as the myocardium, endocardium and cushions/valves and their involvement in
224 congenital heart disease.[22–24] As cardiac innervation follows the developing coronary
225 vasculature,[4,17] here, we specifically focused on expression of the genes in the ventricular
226 innervation and coronaries (Figure 2A). Immunohistochemistry at E18.5 found Slit2 ligand in
227 the endothelium of the coronary veins and arteries, but not in the nerves extending into the

228 heart. At E14.5, Slit3 was neither present in the vessels nor innervation (data not shown), but
229 at E18.5, Slit3 was highly present in the coronary smooth muscle wall and in the larger
230 epicardial nerves, and minimally in intra-myocardial nerves. Both the Robo1 and Robo2
231 receptors were present in the nerves and at low levels in the arteries. Together with the knock-
232 out data, this suggests that the coronary endothelium could act as source of chemo-attractive
233 Slit2 that guides the Robo1-positive nerves during heart development.

234 Therefore, we further focused on the role of Slit2 and knocked-out *Slit2* specifically in
235 the endothelium, which recapitulated the defects seen in the constitutive *Slit2*$^{-/-}$ hearts (Figure
236 2B), which were still visible at E18.5. As Slit2 is also highly expressed in trabecular
237 myocardium, which could act as long-range guidance cue, we additionally removed *Slit2*
238 specifically from the myocardium, which did not show a phenotype compared to wild-type
239 controls at E18.5. While the constitutive double *Robo1/2* knockout did not show an additional
240 role for Robo2 over Robo1 (Figure 1B), this could be caused by Robo2 being expressed in both
241 the endothelium and innervation resulting in opposing signals. We hence deleted *Robo2* in the
242 innervation and endothelium of constitutive *Robo1*$^{-/-}$ mice. *Robo1*$^{-/-}$ hearts showed the same
243 reduction in innervation compared to wild-types as before, which was again not enhanced by
244 specific removal of *Robo2* from the innervation or endothelium (Figure 2B).

245

246 **Reduced sympathetic innervation in absence of endothelial Slit2 limits sympathetic**
247 **stimulation of heart rate**

248 To characterize the type of innervation affected in the endothelial Slit2 knock-out, we
249 specifically quantified sympathetic innervation, which recapitulated the defects seen in the total
250 innervation analysis (Figure 3A-B), showing that endothelial Slit2 guides the sympathetic
251 innervation during heart development. To ensure that endothelial knock-out of Slit2 does not
252 affect coronary vessel formation, we also quantified coronary vessel volumes, showing no

253 difference to controls (Figure 3C-D). Additionally, we validated the specificity of *Slit2* knock-
254 out. Endothelial mutants showed absence of Slit2 from the endothelial cells, however,
255 endocardial expression surrounding the trabeculae was still present (Figure 3E). This is likely
256 caused by secretion of Slit2 from the strongly Slit2 positive trabecular myocardium.[23,24] To
257 further confirm the chemo-attractive role of endothelial Slit2, we cultured wild-type stellate
258 ganglia on their own or in presence of wild-type or endothelial *Slit2* knock-out ventricles.
259 Attraction of axons extending from the ganglia was strongly reduced in the absence of
260 endothelial Slit2 compared to wild-type ventricles (Figure 3F-G). Finally, to confirm functional
261 relevance, we compared heart rate in adult endothelial Slit2 mutants and controls. While
262 baseline heart rates were similar, Slit2 knock-out reduced heart rate increase after sympathetic
263 stimulation with isoproterenol (Figure 3H-I). Combined, this data shows that endothelial Slit2
264 guides sympathetic innervation during heart development and absence results in functional
265 defects.
266
267
268 **Discussion**
269 We have identified an important new chemo-attractive pathway mediated by Slit2 which is
270 required for correct cardiac innervation development. This is somewhat unexpected as Slit2 is
271 mainly known as a chemo-repulsive ligand, repelling extending axons.[28] However, many
272 chemo-active ligands are bifunctional and can promote as well as inhibit axon growth,
273 depending on the circumstances.[36–38] In case of Slit2, it has been shown that concentration
274 levels are important for its bifunctionality as well as proteolytic cleavage, with possible specific
275 biological functions of its N- and C-terminal fragments which are distinct from full-length
276 protein.[39–41] Additionally, the specific chemo-active function of Slit2 can further be modulated
277 by the type of extracellular matrix present.[41] How the attractive function of Slit2 in axon

278 guidance during heart development is regulated will need to be determined. As the endothelial-
279 specific deletion of Slit2 affects endothelial cells throughout the body, the axons extending into
280 the heart could also be influenced before reaching the heart.

281 The increase in innervation in constitutive *Slit3*$^{-/-}$ hearts at E14.5 could suggest that
282 Slit3 has a chemo-repulsive role during early innervation development. However, this effect
283 was not visible anymore around birth and could be caused by the nerves following the abnormal
284 caval vein connections to the heart that are present in this mutant.[24] An indirect effect on
285 innervation is supported by the limited expression of Slit3 in relevant cell-types at E14.5. After
286 E14.5, multiple cell-types start to express Slit3 and the gene also becomes expressed in the
287 large innervation, indicating expression is only turned on as the axons mature. The Slit-Robo
288 pathway is best known for its role during nervous system development, where commissural
289 neurons only become sensitive to repulsive Slit after midline crossing to prevent them from
290 recrossing.[42] A similar temporal activation of the different genes of the pathway in the different
291 cell-types would allow for complex control over where and when axons develop, which will
292 need further investigation. While our data indicates that the innervation responds to endothelial
293 Slit2 through the Robo1 receptor, we also find Robo1 expressed in the endothelium itself. This
294 needs further examination using a conditional Robo1 line, which we failed to generate
295 successfully.[22] These complicated spatio-temporal expression patterns of the genes of the Slit-
296 Robo pathway could be key for determining the sympathetic versus parasympathetic balance
297 or the patterning along veins and arteries.[17,35] Thus, our discovery of an important role for the
298 Slit-Robo signalling pathway during cardiac innervation development raises new exiting
299 questions that will need further investigation.

300

301 **Acknowledgements**

302

Sources of Funding

This work was supported by the British Heart Foundation (PG/15/50/31594), EMBO (ALTF 441-2010), Netherlands Organisation for Scientific Research (825.10.025) and European Research Council (ERC) (715895, CAVEHEART) to MTMM, Oxford BHF Centre of Research Excellence by grant code (RE/18/3/34214) to SB, UKRI-MRC (MR/W006731/1) to KL, BHF FS/19/31/34158 to JV and BBSRC BB/W015277/1 to JV and MTMM.

Disclosures

None

312 **References**

313 1. Mangoni, M. E. & Nargeot, J. Genesis and regulation of the heart automaticity.
314 *Physiol Rev* **88**, 919–982 (2008).
315 2. Ieda, M. & Fukuda, K. Cardiac innervation and sudden cardiac death. *Curr Cardiol Rev*
316 **5**, 289–295 (2009).
317 3. Crick, S. J. *et al.* Innervation of the human cardiac conduction system. A quantitative
318 immunohistochemical and histochemical study. *Circulation* **89**, 1697–1708 (1994).
319 4. Salamon, R. J. *et al.* Parasympathetic and sympathetic axons are bundled in the
320 cardiac ventricles and undergo physiological reinnervation during heart regeneration.
321 *iScience* **26**, 107709 (2023).
322 5. Wagner, J. U. G. *et al.* Aging impairs the neurovascular interface in the heart. *Science*
323 *(1979)* **381**, 897–906 (2023).
324 6. Kapa, S., Venkatachalam, K. L. & Asirvatham, S. J. The autonomic nervous system in
325 cardiac electrophysiology: an elegant interaction and emerging concepts. *Cardiol Rev*
326 **18**, 275–284 (2010).
327 7. Chen, P. S. *et al.* Sympathetic nerve sprouting, electrical remodeling and the
328 mechanisms of sudden cardiac death. *Cardiovasc Res* **50**, 409–416 (2001).
329 8. Chen, P. S., Chen, L. S., Fishbein, M. C., Lin, S. F. & Nattel, S. Role of the autonomic
330 nervous system in atrial fibrillation: Pathophysiology and therapy. *Circ Res* **114**, 1500–
331 1515 (2014).
332 9. Florea, V. G. & Cohn, J. N. The autonomic nervous system and heart failure. *Circ Res*
333 **114**, 1815–1826 (2014).
334 10. Gardner, R. T. *et al.* Targeting protein tyrosine phosphatase σ after myocardial
335 infarction restores cardiac sympathetic innervation and prevents arrhythmias. *Nat*
336 *Commun* **6**, 6235 (2015).
337 11. Vaseghi, M., Lux, R. L., Mahajan, A. & Shivkumar, K. Sympathetic stimulation increases
338 dispersion of repolarization in humans with myocardial infarction. *Am J Physiol Heart*
339 *Circ Physiol* **302**, H1838-46 (2012).
340 12. Miwa, K. *et al.* Axon guidance of sympathetic neurons to cardiomyocytes by glial cell
341 line-derived neurotrophic factor (GDNF). *PLoS One* **8**, e65202 (2013).
342 13. Kimura, K., Ieda, M. & Fukuda, K. Development, maturation, and transdifferentiation
343 of cardiac sympathetic nerves. *Circ Res* **110**, 325–336 (2012).
344 14. Maden, C. H. *et al.* NRP1 and NRP2 cooperate to regulate gangliogenesis, axon
345 guidance and target innervation in the sympathetic nervous system. *Dev Biol* **369**,
346 277–285 (2012).
347 15. Ieda, M. *et al.* Nerve growth factor is critical for cardiac sensory innervation and
348 rescues neuropathy in diabetic hearts. *Circulation* **114**, 2351–2363 (2006).
349 16. Kuruvilla, R. *et al.* A neurotrophin signaling cascade coordinates sympathetic neuron
350 development through differential control of TrkA trafficking and retrograde signaling.
351 *Cell* **118**, 243–255 (2004).
352 17. Poltavski, D. M. *et al.* Venous endothelin modulates responsiveness of cardiac
353 sympathetic axons to arterial semaphorin. *Elife* **8**, 1–23 (2019).
354 18. Ieda, M. *et al.* Sema3a maintains normal heart rhythm through sympathetic
355 innervation patterning. *Nat Med* **13**, 604–612 (2007).
356 19. Blockus, H. & Chédotal, A. Slit-Robo signaling. *Development* **143**, 3037–3044 (2016).

20. Jiang, Z. *et al.* Targeting the SLIT/ROBO pathway in tumor progression: molecular mechanisms and therapeutic perspectives. *Therapeutic Advances in Medical Oncology* vol. 11 Preprint at https://doi.org/10.1177/1758835919855238 (2019).
21. Zhao, J. & Mommersteeg, M. T. M. Slit-Robo signalling in heart development. *Cardiovasc Res* **cvy061**, (2018).
22. Zhao, J., Bruche, S., Potts, H. G., Davies, B. & Mommersteeg, M. T. M. Tissue-Specific Roles for the Slit–Robo Pathway During Heart, Caval Vein, and Diaphragm Development. *J Am Heart Assoc* **11**, (2022).
23. Mommersteeg, M. T. M., Yeh, M. L., Parnavelas, J. G. & Andrews, W. D. Disrupted Slit-Robo signalling results in membranous ventricular septum defects and bicuspid aortic valves. *Cardiovasc Res* **106**, 55–66 (2015).
24. Mommersteeg, M. T. M. *et al.* Slit-roundabout signaling regulates the development of the cardiac systemic venous return and pericardium. *Circ Res* **112**, 465–475 (2013).
25. Andrews, W. *et al.* The role of Slit-Robo signaling in the generation, migration and morphological differentiation of cortical interneurons. *Dev Biol* **313**, 648–658 (2008).
26. Lu, W. *et al.* Disruption of ROBO2 is associated with urinary tract anomalies and confers risk of vesicoureteral reflux. *Am J Hum Genet* **80**, 616–632 (2007).
27. Rama, N. *et al.* Slit2 signaling through Robo1 and Robo2 is required for retinal neovascularization. *Nat Med* **21**, 483–491 (2015).
28. Plump, A. S. *et al.* Slit1 and Slit2 cooperate to prevent premature midline crossing of retinal axons in the mouse visual system. *Neuron* **33**, 219–232 (2002).
29. Gibson, D. A. *et al.* Dendrite self-avoidance requires cell-autonomous slit/robo signaling in cerebellar purkinje cells. *Neuron* **81**, 1040–1056 (2014).
30. Yuan, W. *et al.* A genetic model for a central (septum transversum) congenital diaphragmatic hernia in mice lacking Slit3. *Proc Natl Acad Sci U S A* **100**, 5217–5222 (2003).
31. Danielian, P. S., Muccino, D., Rowitch, D. H., Michael, S. K. & McMahon, A. P. Modification of gene activity in mouse embryos in utero by a tamoxifen-inducible form of Cre recombinase. *Curr Biol* **8**, 1323–1326 (1998).
32. Koni, P. A. *et al.* Conditional vascular cell adhesion molecule 1 deletion in mice: Impaired lymphocyte migration to bone marrow. *Journal of Experimental Medicine* **193**, 741–753 (2001).
33. Sohal, D. S. *et al.* Temporally regulated and tissue-specific gene manipulations in the adult and embryonic heart using a tamoxifen-inducible Cre protein. *Circ Res* **89**, 20–25 (2001).
34. Mommersteeg, M. T. M. *et al.* The sinus venosus progenitors separate and diversify from the first and second heart fields early in development. *Cardiovasc Res* (2010) doi:10.1093/cvr/cvq033.
35. Schneider, C. a, Rasband, W. S. & Eliceiri, K. W. NIH Image to ImageJ: 25 years of image analysis. *Nat Methods* **9**, 671–675 (2012).
36. Wong, J. T. W., Wong, S. T. M. & O'Connor, T. P. Ectopic semaphorin-1a functions as an attractive guidance cue for developing peripheral neurons. *Nat Neurosci* **2**, (1999).
37. De Castro, F., Hu, L., Drabkin, H., Sotelo, C. & Ché Dotal, A. *Chemoattraction and Chemorepulsion of Olfactory Bulb Axons by Different Secreted Semaphorins*. (1999).
38. Colamarino, S. A. & Tessier-Lavigne, M. *The Axonal Chemoattractant Netrin-I Is Also a Chemorepellent for Trochlear Motor Axons*. *Cell* vol. 81 (1995).

39. Pilling, D., Chinea, L. E., Consalvo, K. M. & Gomer, R. H. Different Isoforms of the Neuronal Guidance Molecule Slit2 Directly Cause Chemoattraction or Chemorepulsion of Human Neutrophils. *The Journal of Immunology* **202**, 239–248 (2019).
40. Bhosle, V. K. *et al.* The chemorepellent, SLIT2, bolsters innate immunity against Staphylococcus aureus. *Elife* **12**, (2023).
41. Nguyen-Ba-Charvet, K. T. *et al.* Sensory axon response to substrate-bound Slit2 is modulated by laminin and cyclic GMP. *Molecular and Cellular Neuroscience* **17**, 1048–1058 (2001).
42. Bisiak, F. & McCarthy, A. A. Structure and Function of Roundabout Receptors. in *Macromolecular Protein Complexes II: Structure and Function* 291–319 (2020). doi:10.1007/978-3-030-28151-9_9.

417 **Figures and Figure Legends**

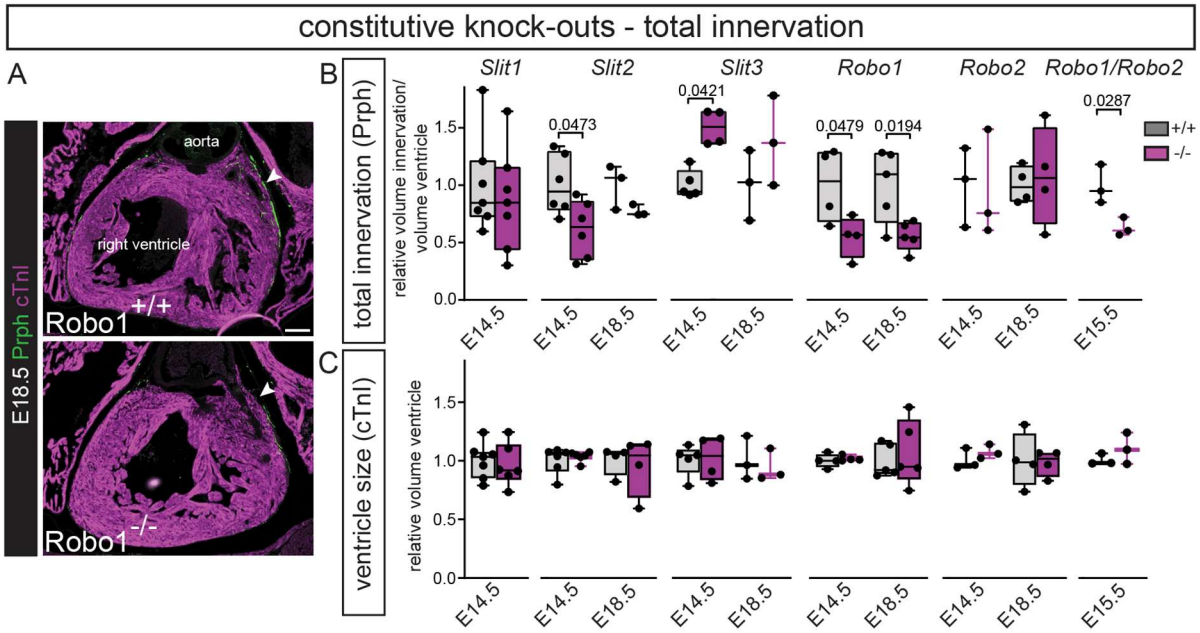

418

419 **Figure 1. Constitutive knock-out analysis indicates a role for Slit2, Slit3 and Robo1**
420 **during cardiac innervation development.** A, Representative images of *Robo1*$^{+/+}$ and *Robo1*$^{-}$
421 $^{/-}$ sections stained by immunohistochemistry for the myocardium using cardiac Troponin I
422 (cTnI) in purple and total innervation using Peripherin (Prph) in green. Arrowhead points to
423 reduced total innervation staining in green in the *Robo1*$^{-/-}$. B, Quantification of total ventricular
424 innervation corrected for ventricle volume (myocardial marker cTnI) in constitutive knock-
425 outs and wild-type controls. T-test or one-way ANOVA with Tukey's Test per mouse line. C,
426 Quantification of total ventricular volume based on myocardial marker cTnI in constitutive
427 knock-outs and wild-type controls. T-test or one-way ANOVA with Tukey's Test per mouse
428 line. Scale bar 100µm.

429

430

431

432

433

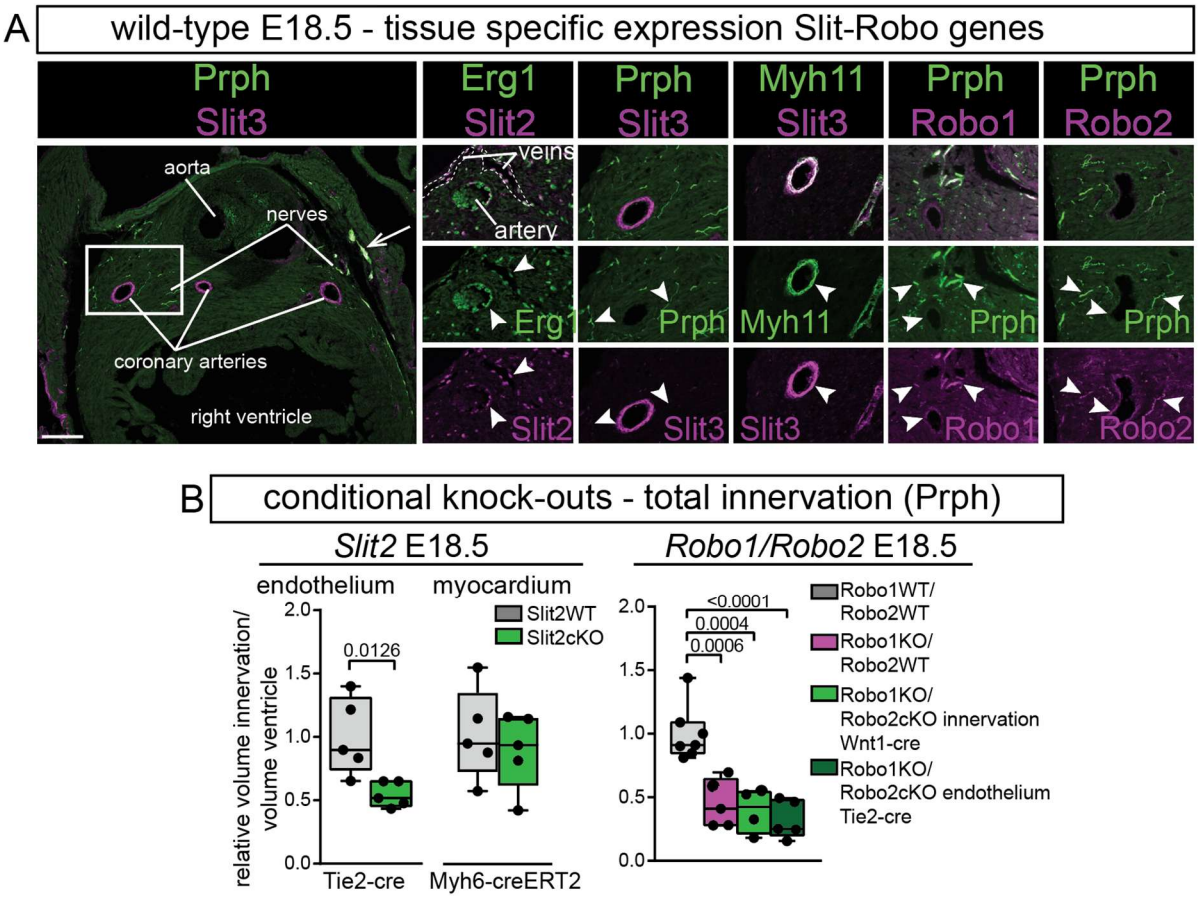

Figure 2. The coronary endothelium acts as source of chemo-attractive Slit2 that guides the Robo1-positive nerves during heart development. A, Immunohistochemistry for Slit2, Slit3, Robo1, Robo2, endothelial marker Erg1, innervation marker Prph and smooth muscle marker Myh11 at E18.5. Box indicates region of magnification. Arrow points to overlap Slit3 and Prph in the large epicardial nerves. White arrowheads point to region of absence or presence of co-localisation of the indicated genes. B. Measurements of total ventricular innervation corrected for ventricle volume in the indicated conditional knock-outs and wild-type controls. T-test or one-way ANOVA with Tukey's Test. Scale bar 100µm.

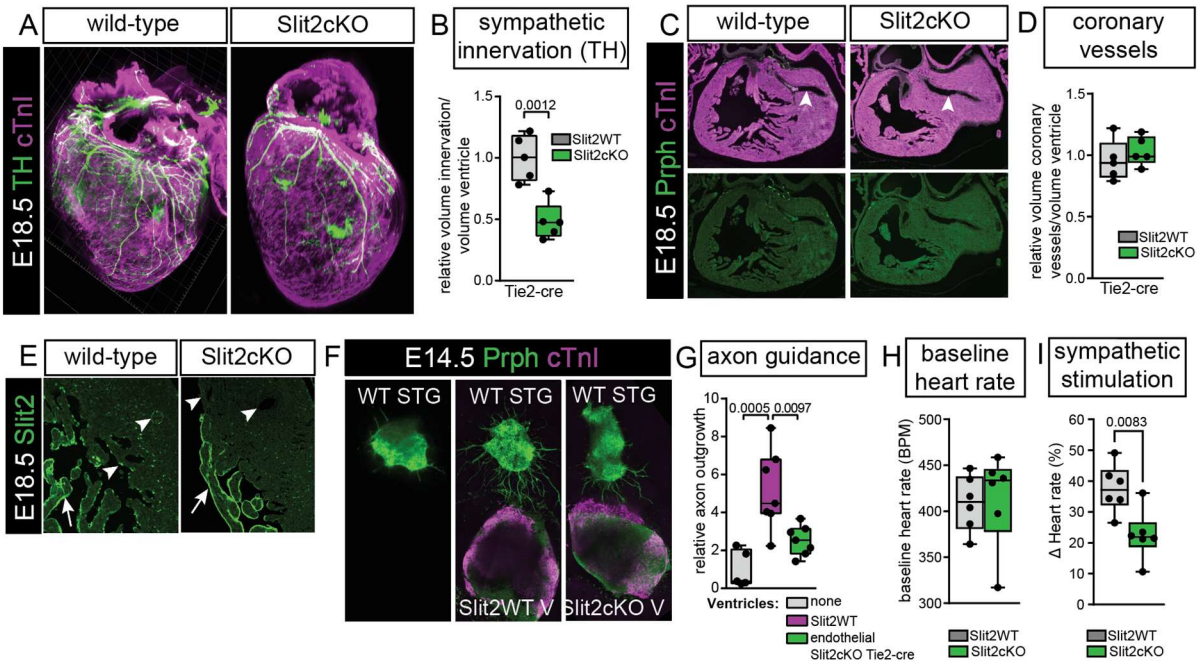

Figure 3. Reduced sympathetic innervation in absence of endothelial Slit2 limits sympathetic stimulation of heart rate. A, Immunohistochemistry for sympathetic innervation marker TH and myocardial marker cTnI on whole mount E18.5 hearts. B, Quantification of sympathetic innervation corrected for ventricle volume in endothelial Slit2 knock-outs versus controls. T-test. C, Immunohistochemistry for total innervation marker Prph and myocardial marker cTnI on E18.5 sections. Arrowheads point to the normal development of the coronary vessels. D, Quantification of coronary vessel volume corrected for ventricle volume in endothelial Slit2 knock-outs versus controls. T-test. E, Immunohistochemistry for Slit2 on endothelial Slit2 knock-outs versus controls, showing the lack of Slit2 in the endothelium. F, E14.5 ventricles and stellate ganglia (STG) cultured in three-dimensional collagen matrix (Chemicon) for 3 days. Immunohistochemistry for Prph and cTnI. G, Quantification of axon outgrowth. One-way ANOVA with Tukey's Test. H, Quantification of baseline heart rate using electrocardiogram. G, Quantification of heart rate after stimulations with isoproterenol. Scale bar 100µm.